# Remote Sensing of Environment

# A review of differential absorption algorithms utilized at NOAA for measuring sea surface temperature with satellite radiometers

CrossMark

Charles C. Walton

*6093 Bahia Del Mar Cir. #476, Saint Petersburg, FL. 33715, United States*

## ARTICLE INFO

## ABSTRACT

In a 1988 study, a generalized non-linear SST algorithm was derived from the radiative transfer equation. An empirical approximation to this algorithm provided the simplified NLSST algorithm for computing sea surface temperatures with satellite radiometer data. It has remained a favorite of the remote sensing community for the past 25 years. However, a 1998 study demonstrated that the functional form of the generalized non-linear algorithm, which is here designated the GNLSST, is very much data dependent. In this paper we explore the various functional forms that the GNLSST may take. Rather than using actual satellite data, we model the effects of atmospheric absorption by water vapor, under saturation conditions, on the satellite split-window temperature difference, ΔT, in the 11–13 μm infra-red spectral region. The parameters used in the GNLSST algorithm are adjusted to demonstrate the various forms that the GNLSST can take. One key finding is that the familiar algorithms used for measuring SST, such as the MCSST, the NLSST and the QSST are all special solutions to the more general GNLSST algorithm. Additionally, the GNLSST may take other forms, which are described graphically.

The simplifying assumptions which yield the NLSST solution represent an approximation to reality when working with actual satellite data. It is demonstrated that minor modifications to the regression procedures, which are used to derive the NLSST with satellite split-window data, may reduce the temperature errors resulting from these approximations. Alternative forms of the GNLSST algorithm may be useful for users of regional split-window satellite data.

## Contents

## 1. Introduction

Anding and Kauth (1970) and Prabhakara et al. (1974) were perhaps the first to suggest the use of multi-spectral data from a radiometer in earth orbit to obtain accurate sea surface temperature measurements (SST) without the need for temperature and humidity profiles of the atmosphere. The idea is that measurements in two or more infra-red

spectral regions (window channels) with differing but small amounts of atmospheric absorption yield a brightness temperature difference, $T_i - T_j$, that is highly correlated to the total temperature deficit in one channel, $T_S - T_i$:

$$T_S - T_i \cong \Gamma * (T_i - T_j) \qquad (1)$$

The parameter, $T_S$, is the sea surface temperature. It was demonstrated that under certain conditions or approximations, which are

*E-mail address:* ccwalton4@hotmail.com.

described in the next section, the gamma parameter, Γ, should be a constant. This approximation has been designated as the multi-channel sea surface temperature algorithm (MCSST).

With the launch of the TIROS (Television Infra-Red Observation Satellite) N series of environmental satellites by NOAA/NESDIS (National Oceanic and Atmospheric Administration)/(National Environmental Satellite Data and Information Service) in 1978, it became possible to test the accuracy of Eq. 1 on a global basis. The AVHRR/2 (Advanced Very High Resolution Radiometer) instrument on the subsequent NOAA 7 satellite provided two channels in the 11–13 μm window spectral region, which enabled the application of the differential absorption technique. Before NOAA-7, attempts were made to correct for the temperature deficit in a single AVHRR window channel measurement using coincident lower resolution TOVS (TIROS Operational Vertical Sounder) atmospheric sounder data, obtained from the same satellite (Cracknell, 1997). These data were applied in a multiple linear regression correction algorithm. These attempts had only limited success, resulting in seasonally dependent biases (Walton, 1982). The differential absorption algorithm (Eq. 1) reduced the errors associated with the previous algorithms by 30% or more! This multiple channel algorithm (MCSST) was applied throughout the 1980s to provide moderately accurate global maps of SST (McClain et al., 1985). Global Comparisons with drifting buoy temperature measurements provide estimates of satellite RMS (root mean squared) temperature errors between 0.6 and 0.7 °C (Strong and McClain, 1984).

Based on the success of the AVHRR instrument, additional instruments have been developed and placed on various international polar orbiting satellite platforms for measuring SST. These include the ATSR (Along Track Scanning Radiometer), MODIS (Moderate resolution Imaging Spectroradiometer), and more recently VIIRS (Visible Infrared Imaging Radiometer Suite), the NOAA replacement for the AVHRR. Each of these instruments has at least two thermal IR (Infra-Red) window channels and one or more mid IR window channels for measuring SST. This paper is concerned with algorithms using only the thermal IR window channels, the so called split-window channels, although the differential absorption algorithms can be applied with a combination of one or more mid IR window channels and a thermal IR window channel.

The term 'error' is applied frequently in this text. When applied to individual channel temperature measurements, it primarily refers to instrumental noise, calibration problems and residual cloud contamination. Some of these errors are correlated between coincident channel measurements and some are not. When the term is applied to split-window SST algorithms, it refers to the ability of the algorithm to correct for atmospheric absorption in the individual channel measurements and provide an accurate estimate of SST. All split-window algorithms tend to magnify the individual measurement errors, some more than others. A useful SST algorithm must provide an accurate correction for the atmospheric absorption while minimizing the effect of the individual channel measurement errors. Validation of SST algorithms involves comparisons with in-situ SST measurements such as provided by drifting buoys in the open oceans. Here, 'error' refers to the bias and scatter of SST algorithm temperature measurements compared to multiple coincident drifting buoy measurements. Validation is not addressed in this study since new satellite data is not analyzed, but it is discussed in many of the references provided in this Introduction.

In the late 1980s, an alternative form of the differential absorption algorithm was developed which is based on less stringent assumptions than the MCSST algorithm (Walton, 1988). This algorithm is of the same form as Eq. 1 but with the gamma parameter having a specific two channel temperature dependence. With simulation and measured temperature data, this new algorithm, designated as the cross product sea surface temperature (CPSST), provided up to a 30% reduction of the errors associated with the MCSST. It replaced the MCSST for operational processing at NOAA in March 1990. It was subsequently empirically found that, with open ocean satellite data, the CPSST gamma parameter could be approximated to be a linear function of the sea surface

temperature. This lead to a simplification of the CPSST, designated as the nonlinear sea surface temperature algorithm (NLSST), (Walton et al., 1990). Because the NLSST algorithms further reduced the temperature errors associated with global data sets of satellite measurements compared to the CPSST and MCSST, it was made operational in April 1991. It has remained a favorite of the international SST remote sensing community for the past 25 years and is currently being used with the VIIRS instrument.

Over the years, there have been many developments in the application of the NLSST including how the coefficients, such as shown with Eq. 19, are derived. In the original formulation it is assumed one set of coefficients applies globally (Walton et al., 1998). Modifications of the NLSST approach include:

(1) stratifying coefficients as a function of $T_i - T_j$ (Kilpatrick et al., 2001; Minnett et al., 2004), (2) stratifying coefficients by zonal bands and by month (Minnett, 1990; Minnett and Evans, 2009), (3) including a satellite zenith angle dependence for most coefficients (Le Borgne et al., 2013), (4) adding an offset to the initial estimate of sea surface temperature, $SST_0$, used to define the NLSST gamma parameter (Hosoda and Qin, 2011, and Cayula et al., 2013).

A further discussion of these modifications is given in Petrenko et al. (2014). The benefits of adding an offset to the initial SST estimate is discussed in Section 6. The first three modifications are intended to reduce regional biases associated with the NLSST, which are present to some degree in any global split-window algorithm as is explained in Merchant et al. (2008). Another technique for reducing regional biases is the application of Optimal Estimation. This procedure can be considered to dynamically derive regression coefficients based on prior knowledge of the atmosphere such as provided by numerical weather prediction fields (Merchant et al., 2008). These refinements are beyond the scope of this paper. To the extent that the NLSST and the GNLSST algorithms reduce regional biases compared to the MCSST, the weight that must be assigned to the a priori data to eliminate these biases is also reduced.

The success of the NLSST algorithm is definitely data dependent. A 1998 study used two data sets. One consists of a 115 simulated split-window channel measurements, computed at nadir, derived from radiosonde atmospheric temperature and moisture profiles which are applied in a Radiative Transfer Model (Weinreb and Hill, 1980). With this data set, the NLSST provides no improvement over the MCSST while the CPSST algorithm provides a 30% improvement in the estimation of SST when compared to the other algorithms. Most surprisingly, the temperature dependence of the CPSST gamma parameter varied greatly, depending on which data set is used to develop the CPSST algorithm. A second data set consists of actual open ocean satellite data, including some 4000 match-ups with drifting buoy measurements made at various zenith angles up to $53^0$. With the open ocean data, the gamma parameter may be approximated as a linear function of the surface temperature while with the simulation data it is best approximated as a linear function of the window channel temperature difference (Walton et al., 1998). This latter solution is referred to as the quadratic sea surface temperature algorithm (QSST) since the temperature correction is a quadratic function of the measured temperature difference. This form of solution has been suggested previously (McMillin, 1975).

These results beg the question of what other forms the CPSST algorithm may take when developed with different data. The answer to this question is the primary goal of this research. Rather than applying actual temperature data to describe the variation in atmospheric absorption in the window channels, a mathematical model is developed to describe the maximum and minimum absorption likely to exist in actual data. In this study, it is demonstrated that both the MCSST and the NLSST algorithms are special solutions of the more general CPSST algorithm. The CPSST designation originated from a geometric derivation provided in the 1988 study. Because both the MCSST and the NLSST as well as the QSST are special solutions of the more general algorithm, it is perhaps more appropriate

to designate it as the Generalized Non Linear Sea Surface Temperature algorithm (GNLSST). This is done in the remainder of this text. An explanation for the different results obtained with the open ocean and simulation data is provided and possible improvements to both the GNLSST and NLSST algorithms are suggested.

## 2. Derivation of differential absorption algorithms from radiative transfer theory

The measured radiance at the top of the atmosphere at wave number $\nu$, I ($\nu$), is composed of an emitted surface term, which is partially absorbed by the atmosphere, and an atmospheric term representing the net emission minus absorption of each pressure layer of the atmosphere:

$$I(\nu) = B(\nu, T_S) * \tau + \int_{\tau}^{1} B(\nu, T_P) d\tau \tag{2}$$

This simplified form of the radiation transfer equation is applicable in the 11–13 μm spectral region because the sky and solar reflected radiation is assumed to be negligible compared to the emitted surface radiation and the ocean surface is very nearly a blackbody (Smith et al., 1974). It should be noted that these assumptions are not valid for measurements made at large satellite zenith angles resulting in an over estimation of I($\nu$) with Eq. 2 (Dash and Ignatov, 2008).

In this equation, B is the Planck radiance which is a function of wave number and temperature and $T_S$ is the temperature of the ocean surface. This equation states that the net radiation at wave number $\nu$, measured at the top of the atmosphere, consists of a surface emitted Planck radiance, $B(\nu, T_S)$, which is partially absorbed by the atmosphere, plus a summation of the net emission minus absorption of radiance by each layer of the atmosphere. This summation is a function of the concentration of the atmospheric constituents as well as the temperature at each pressure level in the atmosphere, $T_P$. With the mean value theorem of calculus, Eq. 2 can be simplified to the form:

$$I(\nu) = B(\nu, T_S) * \tau + B(\nu, T^a) * (1 - \tau) \tag{3}$$

In Eq. 3, $T_S$ is the surface temperature, $\tau$ is the transmittance from the surface to the top of the atmosphere and $T^a(\nu)$ is the temperature at some level of the atmosphere chosen so that the second terms of Eqs. 2 and 3 are equal. A series of approximations are now performed which is described by McMillin and Crosby (1984). First, because water vapor absorption in the 11–13 μm spectral region occurs primarily in the lowest layers of the atmosphere, one may perform a Taylor series expansion of Eq. 3 about $T_S$ to convert from radiance units to temperature units. (As is explained in Minnett, 1986, neglecting the interaction between the IR radiation and water vapor molecules higher in the atmosphere may be questionable because proportionally these interactions are more important to the atmospheric effect.) Second, water vapor transmittance for a radiometer window channel i, can be approximated with $\tau_i = 1 - k_i * w$ where w is the water vapor concentration in a column of the atmosphere and $k_i$ is the absorption coefficient of that channel. These approximations yield the following equations for two channels in the 11–13 μm spectral region:

$$\begin{aligned} T_i &= T_S - k_i * b_i \\ T_j &= T_S - k_j * b_j \end{aligned} \tag{4}$$

In this equation, $T_i$ is the channel i measured temperature and $b_i = w * (T_S - T_i^a)$. Eq. 4 applies to one satellite measurement made in two window channels and the water vapor concentration,

w, will vary with each measurement. The MCSST solution is obtained from this set of linear equations under the assumptions that $k_i$ and $k_j$ are constants and the atmospheric temperatures, $T_i^a$ and $T_j^a$, are equal, yielding:

$$MCSST = T_i + \Gamma * (T_i - T_j) \tag{5}$$

The parameter $\Gamma = k_i / (k_j - k_i)$. The viability of this last assumption is a source of controversy and is discussed in McMillin and Crosby, 1984.

In general $b_i$ and $b_j$ vary with each atmosphere and cannot be obtained from satellite measurements. One can however define an average $\overline{b}_i$ and $\overline{b}_j$ with an ensemble of data subject to the condition that the measured temperature $T_i$ or $T_j$ is constant. With this subset of data, Eq. 4 yields:

$$\begin{aligned} \overline{T}_S(T_i) &= T_i + k_i * \overline{b}_i(T_i) \\ \overline{T}_S(T_j) &= T_j + k_j * \overline{b}_j(T_j) \end{aligned} \tag{6}$$

The mean surface temperature estimates are channel dependent because the ensemble of data used to compute the means is different with each channel. In addition to the channel dependence, there is an instrumental dependence, resulting from the different relative spectral response functions of the same channels on different instruments (P.J. Minnett, personal communication). Subsequently these single temperature estimates will be designated as $SST_i$ and $SST_j$. Eq. 6 defines the absorption coefficients as a function of the single channel temperature measurements and substituting these expressions into Eq. 4, one obtains the following set of equations:

$$\begin{aligned} T_i &= T_S - (SST_i - T_i) * b_i / \overline{b}_i(T_i) \\ T_j &= T_S - (SST_j - T_j) * b_j / \overline{b}_j(T_j) \end{aligned} \tag{7}$$

Assuming $b_i / \overline{b}_i = b_j / \overline{b}_j$, Eq. 7 represents two equations with two unknowns resulting in the following solutions:

$$GNLSST = T_i + \frac{SST_i - T_i}{SST_j - T_j + T_i - SST_i} * (T_i - T_j) \tag{8}$$

$$b_i / \overline{b}_i = (T_i - T_j) / (SST_j - T_j + T_i - SST_i) \tag{9}$$

It should be noted that the GNLSST solution involves less restrictive assumptions than the MCSST. Most notably, the mean atmospheric temperatures, $T_i^a$ and $T_j^a$ need not be equal. However, even if the MCSST assumptions were correct, the GNLSST would still represent a viable alternative solution for the measurement of SST. The difference between these solutions results from the application of the single channel algorithms, $SST_i$ and $SST_j$ in the GNLSST formalism. These algorithms are insensitive to variable water vapor absorption at a fixed temperature, providing only a mean correction. However they are sensitive to temperature dependent effects such as the saturation water vapor concentration of the atmosphere as well as absorption by uniform gases. These physical effects are completely excluded in the MCSST derivation. It is interesting that these single temperature algorithms, which were originally used in the 1970s to provide approximate estimates of SST, are here used to describe the temperature dependence of the gamma parameter in the GNLSST formalism. With Eq. 8, it is observed that if the single channel temperature estimates are equal then the GNLSST is identical to the single channel estimate, $SST_i$. With Eq. 9 it is seen that this only occurs in a typical or climatological atmosphere when $b_i = \overline{b}_i$. In an atypical atmosphere, the two single channel solutions diverge, and the multichannel GNLSST solution provides the greater accuracy.

Before one can apply the GNLSST algorithm, the single channel SST estimates, $SST_i$ and $SST_j$, must be specified. A simple linear expression

is sufficient for this purpose:

$$SST_{11} - T_{11} = S_{11} * T_{11} + I_{11}$$
$$SST_{12} - T_{12} = S_{12} * T_{12} + I_{12} \qquad (10)$$

In this equation, $S_I$ and $I_I$ represent the slope and intercept coefficients for the 11 and 12 μm channels. With open ocean satellite data, these coefficients can be obtained by linear regression using a data set of coincident buoy SST measurements and satellite radiometer temperature measurements. These coefficients can also be obtained with simulation data derived from a radiative transfer model (May and Holyer, 1993; Walton et al., 1998).

## 3. Modeling the atmospheric water vapor absorption in the 11-13 μm window spectral region

Based on the previously cited 1988 and 1998 studies with data sets of simulated and actual satellite measurements, it is possible to estimate the maximum and minimum atmospheric absorption in the split-window channels used in the differential absorption algorithms. Specifically, it is assumed that the maximum temperature difference between coincident split-window measurements, $\Delta T$, can be modeled as a function of the temperature measurement in one channel, $T$, over a range from 0 to 30 °C. A cubic equation is assumed to be adequate for this purpose:

$$\Delta T_{max} = a + b * T + c * T^2 + d * T^3 \qquad (11)$$

The coefficients are defined by specifying three points along the curve. The following physical restraints help to specify these points:

(1) The saturation water vapor concentration is temperature dependent, approaching zero as the atmospheric temperature approaches 0 °C (Stephens, 1990).
(2) Bulk open ocean temperatures achieve a maximum of approximately 30 °C over the earth, based on buoy and ship measurements (see Figs. 4 & 5 in Hosoda and Qin, 2011). This limit is a consequence of heat budget considerations. Radiant solar heating is balanced by ocean mixing between the surface and the bulk, evaporative ocean cooling and surface infra-red radiant emission. Consequently, satellite temperature measurements approaching 30 °C should only occur in very dry or near isothermal atmospheric conditions with $\Delta T$ restrained to very small values.
(3) The maximum temperature difference between split-window channel measurements, found in both a global set of cloud free data and a simulation data set, is approximately 3 °C occurring at satellite measured temperatures between 20 and 25 °C (see Figs. 2 & 3 in Walton et al., 1998 and Figs. 3 & 4 in Walton, 1988). The exact value is instrument dependent since each instrument has slightly different spectral response functions for the same split-window channels.

Exceptions to these restraints will occur under unusual atmospheric or sea state conditions such as strong diurnal solar heating of the near surface ocean layers when the sea is calm and large air-sea temperature differences which can occur near coastlines. A combination of high solar insolation and low wind speed can result in a diurnal variation of SST of 1 °C or more (Webster et al., 1996). Surface air-sea temperature differences of 10 °C or more provide similar variations in satellite measured SST and are algorithm dependent (May and Holyer, 1993). However, these conditions are rare and transitory by nature.

Based on the prior restraints, the following three points define a curve:

$\Delta T_{max} = 0$ at the temperature extremes, $T = 0$ and $T = 30$ °C and $\Delta T_{max}$ attains a maximum value of 3 at $T = 20$ °C yielding:

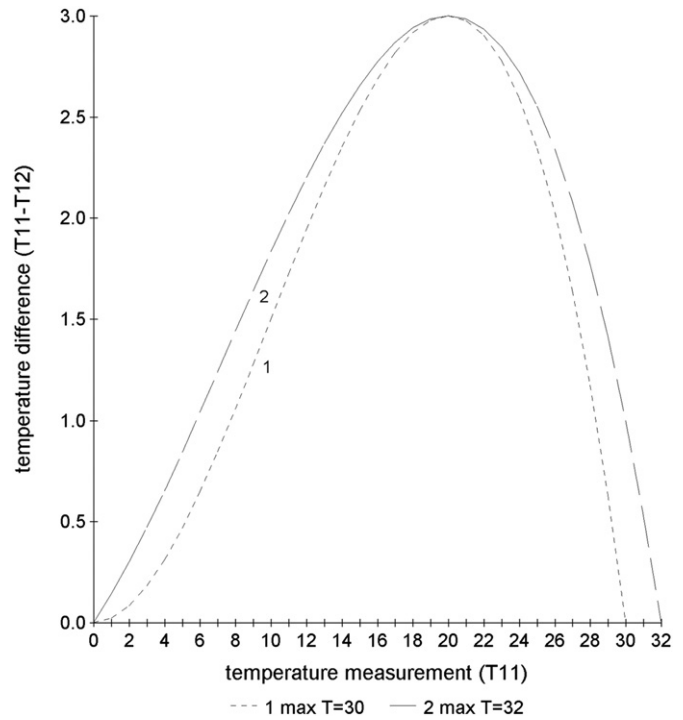$$\Delta T_{max} = 9/400 * T^2 - 3/4000 * T^3 \qquad (12)$$



**Fig. 1.** The maximum $(T_{11} - T_{12})$ vs. $T_{11}$. The maximum temperature difference is modeled using two criteria. Curve 1 assumes a maximum sea surface temperature of 30 °C while curve 2 assumes a value of 32 °C.

This curve is shown in Fig. 1. Different curves could be derived consistent with the general restraints described previously. A second curve shown in Fig. 1 uses the same criteria as above except that the maximum surface temperature is assumed to be 32 °C. Obviously, there is a family of curves which satisfy the general criteria given above. Eq. 12 has been chosen somewhat arbitrarily due to its simplicity. In general, details such as the appropriate value of $\Delta T$ at the temperature extremes, zero or a small positive or negative value, as well as the measured temperature at which $\Delta T$ achieves its maximum value, 20 to 25 °C, are inconsequential to the results obtained in this study.

The minimum temperature difference, $\Delta T_{min}$, is easier to define. Water vapor concentration is highly variable and can be near zero even in a hot atmospheric environment. Additionally, even in moist atmospheres, if the atmospheric temperature profile is near isothermal, there will be no net atmospheric absorption. Therefore, $\Delta T_{min}$ is approximately zero over the entire ocean temperature range. These parameters, $\Delta T_{min}$ and $\Delta T_{max}$ will be applied to various GNLSST algorithms, as described in the following sections, to demonstrate the temperature and water vapor dependence of the associated gamma parameters.

It is also useful to determine the variation of the gamma parameter as a function of $\Delta T$. For this purpose it is necessary to determine the minimum and maximum temperatures associated with a given value of $\Delta T$ which is consistent with Eq. 12. This requires solving the cubic Eq. 12 for different values of $\Delta T$. The solution yields three values for temperature, one of which is imaginary. The remaining two values represent minimum and maximum temperatures associated with a given value of $\Delta T$. The following table provides this information:

**Table 1**
The minimum and maximum temperature solutions to Eq. 12 as a function of $\Delta T$.

| $\Delta T$ | 0 | 0.25 | 0.5 | 0.75 | 1 | 1.25 | 1.5 | 1.75 | 2 | 2.25 | 2.5 | 2.75 | 3 |
|---|---|---|---|---|---|---|---|---|---|---|---|---|---|
| T1 | 0 | 3.6 | 5.2 | 6.5 | 7.7 | 8.9 | 10 | 11.1 | 12.3 | 13.5 | 14.8 | 16.5 | 20 |
| T2 | 30 | 29.6 | 29.2 | 28.8 | 28.3 | 27.9 | 27.3 | 26.7 | 26.1 | 25.3 | 24.4 | 23.2 | 20 |

The values $\Delta T_{max}$ and $\Delta T_{min}$ represent the extreme effects of variable water vapor absorption on satellite window channel measurements. Each of these values may be applied to the GNLSST gamma parameter, defined with Eq. 8, to obtain a curve representing the GNLSST gamma parameter as a function of temperature. These two curves form an envelope which specifies the maximum scatter in gamma resulting from variable water vapor concentrations. Nearly all individual satellite measurement of gamma should be within this envelope. Similarly, the maximum scatter of gamma as a function of $\Delta T$ is defined by substituting the temperatures T1 and T2, given in Table 1, into the GNLSST gamma parameter. The resulting two curves as a function of $\Delta T$ form an envelope which should encompass nearly all the individual satellite measurements of gamma. These effects are demonstrated with Figs. 2 and 3. These figures show two envelopes. The top envelope is derived as described above, using a data set consisting of 115 simulated satellite measurements, which is described in the Introduction. This data set is used to derive the single channel algorithms, $SST_{11}$ and $SST_{12}$. The sea surface temperature is assumed to be equal to the radiosonde surface air temperature measurement although, over nearly all of the oceans, the SST is slightly warmer than the surface air temperature (P. Minnett, personal communication). The bottom envelope is derived using actual satellite measurements coincident with drifting buoy measurements of sea surface temperature to define the single channel algorithms. The envelopes are separated by a value of 1 on the ordinate scale to separate the data. The actual single channel algorithms, $SST_{11}$ and $SST_{12}$, are obtained from the equations provided in the 1998 study. The individual data points are derived from individual radiosonde temperature and moisture profiles and are obtained from the relevant figures provided in the 1998 study. The data points are superimposed over the appropriate envelopes to produce the results shown in Figs. 2 and 3. It is seen that a large majority of the 115 data points fall within the envelopes providing a proof of concept for the modeling procedure developed in this study. These data are not representative of a global data set and are included for illustrative purposes only. Most of the outliers are in cold temperature regions where the simulated satellite temperature measurements may be below 0 °C (negative temperatures are not included in the derivation of the envelopes shown in Figs. 2 & 3).

It should be noted that the simulated temperature measurements, $T_{11}$ and $T_{12}$, derived from each of the radiosonde profiles, using the radiative transfer Eq. 2, are identical in the upper and lower envelopes of these figures. It is only the single channel algorithms, $SST_{11}$ and $SST_{12}$, which provide the obvious differences in the dependence of the gamma parameter upon the temperature difference, $T_{11}$-$T_{12}$, and the sea surface temperature.

During the review process, it has been suggested that a much larger simulation data set, computed using modern radiative transfer calculations, and including a greater range of atmospheric and moisture conditions should be applied here. Although beyond the scope of this research effort, I would concur with this assessment with one caveat. Although small in numbers, derived from 115 radiosonde soundings over open oceans, the 1998 simulation data set of satellite radiometer temperature measurements includes a wide range of moisture and temperature conditions around the world. Historically, this type of simulation data set was used at NOAA during the 1980s to compute operational MCSST algorithms due to the lack of buoy temperature measurements in the open oceans. The limited number of buoy-satellite temperature match-ups that were available provided a temperature dependent bias correction to the simulation MCSST algorithms (Strong and McClain, 1984). Modern satellite simulations are much more extensive and more accurate then were the simulations used at NOAA in the 1980s and 1990s. The modeling of ocean surface emissivity as a function of satellite zenith angle in modern radiative transfer models allows for the simulation of satellite measurements over the entire scan of the radiometer. Rather than using radiosonde soundings to provide the temperature and moisture profiles of the atmosphere, a modern RTM obtains this data from a Global Data Assimilation System (GDAS)
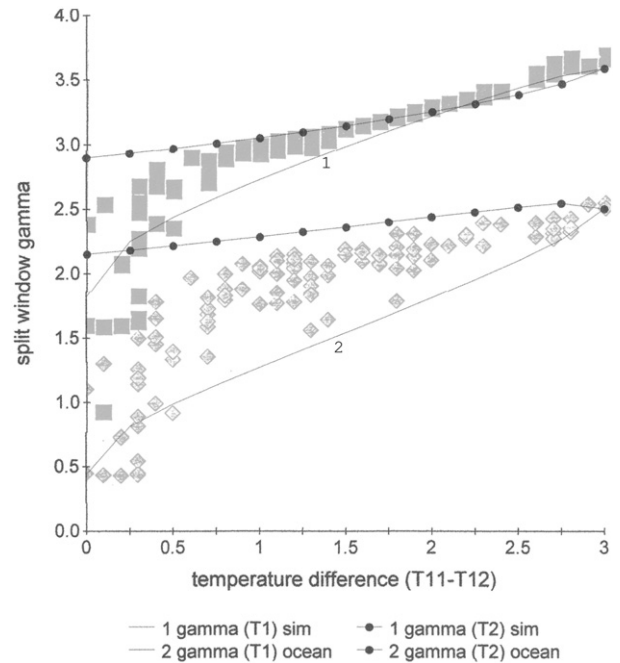


**Fig. 2.** GNLSST gamma vs. $T_{11} - T_{12}$. Envelope #1 is obtained from single channel slope and intercept parameters derived from simulation data described in the 1998 study. Envelope #2 is obtained from parameters derived from NOAA 14 AVHRR satellite ocean temperature measurements described in the same study. The individual data points were obtained in the same study from radiosonde atmospheric temperature and humidity measurements applied in a radiative transfer model. In this and subsequent figures, the parameters T1 & T2 represent the minimum and maximum temperatures associated with a given value of $T_{11} - T_{12}$ as shown in Table 1 of the text. A value of one has been added to the envelope #1 data to separate the two data sets.
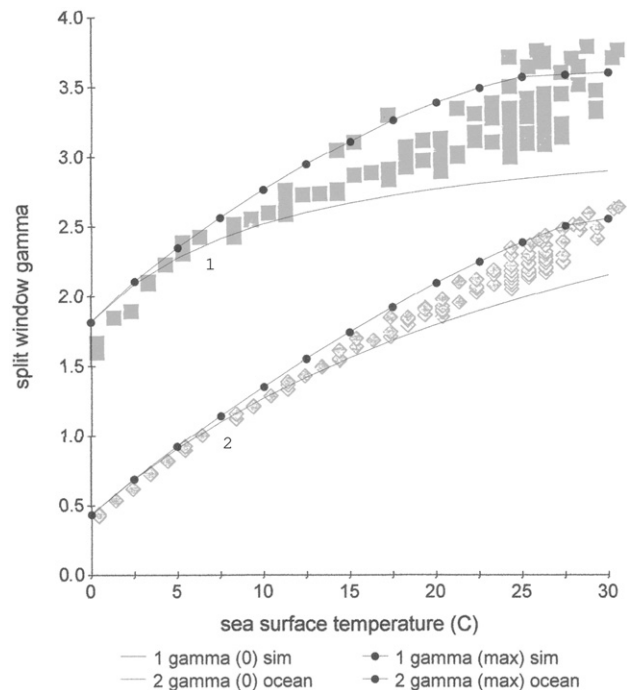


**Fig. 3.** GNLSST gamma vs. SST. Envelope #1 is obtained from single channel slope and intercept parameters derived from simulation data described in the 1998 study. Envelope #2 is obtained from parameters derived from NOAA 14 AVHRR satellite ocean temperature measurements. The individual data points were obtained in the same study from radiosonde atmospheric temperature and humidity measurements applied in a radiative transfer model. In this and subsequent figures, gamma (0) and gamma (max) are the values obtained when $T_{11} - T_{12} = 0$ and $T_{11} - T_{12}$ is the maximum for a given value of $T_{11}$ as is depicted in Fig. 1. A value of one has been added to the envelope #1 data to separate the data.

maintained by the National Weather Service (Dash and Ignatov, 2008). Consequently satellite radiometer temperature simulations can be computed globally over all ocean locations. If this capability had existed at the time of the 1998 study, then a simulation data set, similar in terms of the number and data distribution to the approximately 4000 open ocean buoy-satellite match-up data set, could have been applied. In that case, the data dependence of the GNLSST solution may not have been observed and a major incentive for the current study, to examine that dependence, would not have existed. Today, modern satellite simulation data is used extensively at NOAA to monitor biases in satellite derived clear-sky window channel temperature measurements and sea surface temperatures (Liang and Ignatov, 2011). In the Conclusion, it is suggested that regional users of satellite data might consider the application of regional GNLSST algorithms for measuring sea surface temperature. The application of modern satellite simulation data in the study of various regional GNLSST algorithms as well as in the computation of sea surface temperatures using a global GNLSST algorithm may provide new research opportunities.

The various curves and envelopes shown here and in the following sections are based on calculations performed at specific temperature ($T_{11}$) intervals or temperature difference ($T_{11}$–$T_{12}$) intervals. Although any interval value could be applied, a temperature interval of 2.5 °C is adopted over the range from 0 °C to 30 °C. Similarly a temperature difference interval of 0.25 °C is applied over the temperature difference range from 0 to 3 °C. At each interval, all the relevant parameters are computed. This includes the minimum and maximum $T_{11}$ or $T_{12}$ values derived from Eq. 12 or Table 1, and the single channel sea surface temperature values, $SST_{11}$ and $SST_{12}$. These values define the associated minimum and maximum gamma parameters curves and envelopes, which are discussed in the subsequent sections.

## 4. Behavior of the GNLSST gamma parameter under special conditions

In the following section the behavior of the gamma parameter will be examined as the slope and intercept parameters, as defined with Eq. 10, are varied. In this section, special conditions are considered mathematically. Substituting Eq. 10 into Eq. 8 one obtains the following expression for the GNLSST gamma parameter:

$$\Gamma = (S_{11} * T_{11} + I_{11})/(S_{12} * T_{12} - S_{11} * T_{11} + I_{12} - I_{11}) \qquad (13)$$

Generally, these slope and intercept parameters, obtained by linear regression using a global data set of independent SST measurements and coincident satellite radiometer measurements, have small positive values. Certain combinations of these parameter values result in special types of algorithms which are examined here.

Type 1: The MCSST approximation: $S_{11} = S_{12} = 0$.

In this case, gamma = $I_{11}$ / ($I_{12} - I_{11}$). Gamma is a constant, independent of temperature or water vapor absorption, which is the MCSST approximation. This is generally a bad approximation because of the strong water vapor saturation temperature dependence. This results in low water vapor concentrations in polar regions (0.5 cm precipitable water) compared to tropical regions (5 cm precipitable water on average) (Stephens, 1990). Consequently, there is much less water vapor absorption at low temperature than at higher temperatures on average, which results in positive slope parameters. Other effects such as a temperature dependence of the absorption coefficients ($k_{11}$ & $k_{12}$) are minor compared to the atmospheric water vapor saturation effect. However, regional users of satellite data with limited temperature variation such as in the tropics might obtain slope values that are near zero or even negative as is described in the Conclusion.

Type 2: The single channel approximation: $S_{11} > 0$; $S_{12} = 0$ or $S_{11} = 0$; $S_{12} > 0$.

In this case, gamma is a function of a single channel temperature measurement. It is difficult to imagine a situation in which these conditions would apply to global data sets. Nevertheless, this possibility is

included in the graphical discussion in the following section for completeness and comparison purposes and is demonstrated with Figs. 8 & 14.

Type 3: The water vapor atmosphere approximation: $I_{11} = I_{12} = 0$.

In this case, gamma = $S_{11} * T_{11}$ / ($S_{12} * T_{12} - S_{11} * T_{11}$). The gamma value for the low water vapor curve of the envelope, i.e. $T_{11} = T_{12}$, is given by, gamma = $S_{11}$ / ($S_{12} - S_{11}$), a constant. This condition might apply if water vapor was the only absorbing constituent in the atmosphere since water vapor absorption falls to near zero in polar atmospheres.

Type 4: $S_{11} = a * I_{11}$; $S_{12} - S_{11} = b * (I_{12} - I_{11})$ and a = b.

In this case, the gamma value for the low water vapor curve is given by, gamma = $I_{11}$ / ($I_{12} - I_{11}$) = $S_{11}$ / ($S_{12} - S_{11}$), a constant. Thus, one obtains the same result as in the previous case without the intercept parameters being zero. A demonstration of the resulting envelope curves is shown in Fig. 7. Generally, the ratio, R = b / a, is a variable which provides information regarding the nature of the GNLSST algorithm. If R is greater than unity then the gamma parameter decreases with increasing temperature, at least over a portion of the temperature range, while a negative value implies that the slope $S_{12}$ is less than $S_{11}$. This is unexpected since water vapor absorption is greater in the 12 μm spectral region than in the 11 μm region. Solutions with R in the most physically interesting range between 0 and 1 are demonstrated in the following section. Additionally solutions with $R < 0$ are also considered for completeness of the analysis.

Type 5: The NLSST approximation: $S_{12} = S_{11} > 0$.

Substituting Eq. 10 into Eq. 8 and assuming $S_{11} = S_{12}$, it is readily shown that the GNLSST and its associated gamma parameter are given by:

$$GNLSST = \{I_{11} * (T_{11} - T_{12}) + T_{11} * (I_{12} - I_{11})\}/\{S_{11} * (T_{12} - T_{11}) + I_{12} - I_{11}\} \qquad (14)$$

$$\Gamma = (S_{11} * T_{11} + I_{11})/\{S_{11} * (T_{12} - T_{11}) + I_{12} - I_{11}\} \qquad (15)$$

When $S_{11} = S_{12}$, it can be proven that the GNLSST algorithm simplifies to the familiar NLSST. The NLSST formalism requires that gamma is a linear function of the sea surface temperature:

$$NLSST\ gamma = c * GNLSST + d. \qquad (16)$$

It is easily shown that, with the following values for the coefficients, Eq. 15 and 16 are identical, verifying the assertion:

$$c = S_{11}/(I_{12} - I_{11}); \quad d = I_{11}/(I_{12} - I_{11}) \qquad (17)$$

It has been demonstrated in this section that, under specific conditions, the GNLSST degenerates into either the familiar MCSST or NLSST algorithm. Certainly, the conditions for the NLSST formalism are less restrictive than that for the MCSST. As has been stated previously, the NLSST algorithm has been a favorite of the sea surface temperature remote sensing community for the past 25 years. Nevertheless, the NLSST is an approximation of the more general GNLSST. With both simulation and open ocean satellite data sets it has been found that the slope $S_{12}$ is somewhat greater then $S_{11}$, as should be expected since the water vapor absorption is greater in the 12 μm spectral region. (In the Conclusion, it is demonstrated that this statement may not apply to regional or local scale data sets in which the temperature range of the data is limited.)

Type 6: The QSST approximation.

Fig. 2 plots the GNLSST gamma parameter, derived from a simulation data set described in the 1998 study, as a function of the temperature difference, $T_{11} - T_{12}$. The high and low temperature curves, as defined with Table 1, cross at the intermediate value of $T_{11} - T_{12} = \Delta T_C = $ 2.1. At this point, the gamma parameter is a constant independent of the $T_{11}$ temperature. Because the curves cross, the envelope of allowable gamma values, as a function of $T_{11} - T_{12}$, is very restrictive and the

gamma parameter may be approximated as a linear function of the temperature difference, $T_{11} - T_{12}$. This approximation yields the Quadratic Sea Surface Temperature Algorithm (QSST) where the SST is a quadratic function of $T_{11} - T_{12}$ (Kumar et al., 2003). It is useful to consider under what conditions the GNLSST approximates the QSST. Equating the GNLSST gamma parameters, defined with Eq. 13, when $T_{11} - T_{12} = \Delta T_C$, at two different temperatures values, $T_{11}$, between the extremes listed in Table 1, one obtains:

$$I_{12} - I_{11} = \Delta T_C * S_{12} + I_{11} * (S_{12} - S_{11})/S_{11} \qquad (18)$$

Given values for the slope and intercept values ($S_{11}$, $S_{12}$ and $I_{11}$), which can be obtained from either a simulation or open ocean data set, Eq. 18 defines a value for the intercept, $I_{12}$, such that the QSST approximation may apply. The resulting algorithm may or may not be useful for estimating SST, depending on the magnitude of the associated gamma parameter. Substituting Eq. 18 into Eq. 13, one finds gamma = $S_{11} / (S_{12} - S_{11})$ at the point that the envelope curves cross, $T_{11}-T_{12} = \Delta T_C$. It is seen that gamma is a strong function of the difference in slope values, $S_{12} - S_{11}$. It is perhaps remarkable that the slope and intercept parameters obtained from the simulation data sets developed in both the 1998 and 1988 studies, with $S_{12} - S_{11} = 0.06$, are such that the optimal GNLSST algorithm approximates the QSST formulation. This is not the case when the parameters are derived from the open ocean satellite data set with $S_{12} - S_{11} = 0.04$.

Type 7: The uniform surface temperature approximation $S_{11} < 0$; $S_{12} < 0$.

The previous types of solutions may occur in global data sets in which there is a large range of surface temperatures and satellite temperature measurements. Type 7 solutions may occur in regional or local scale data sets in which the variation in satellite temperature measurements due to variable water vapor absorption may be greater than the variation in sea surface temperature. In the limit that the SST is a constant within a given data set, it is easily verified that a linear regression will yield the slope parameters, defined with Eq. 10, $S_{11} = S_{12} = -1$ and the intercept parameters $I_{11} = I_{12} =$ the constant SST. Thus, in this limit, the GNLSST solution degenerates to the constant SST, independent of the satellite temperature measurements $T_{11}$ and $T_{12}$. The associated gamma parameter becomes an inverse function of the temperature difference, $T_{11} - T_{12}$. An example of this type of solution is provided in the Conclusion.

## 5. A graphical description of the GNLSST gamma parameter as slope and intercept parameters are varied

It is desired to show graphically the behavior of the GNLSST gamma parameter as the single channel slope and intercept parameters, defined with Eq. 10, are varied. In the 1988 and 1998 studies these parameters are derived from data sets of simulated or actual satellite measurements in the 11 μm and 12 μm spectral intervals. In this study one may freely vary these parameters since actual satellite measurements are not utilized. However, restrictions are placed on the parameters to insure that the resulting solutions are realistic. The 11 μm single channel slope and intercept values are not varied. The values for these parameters are taken from the 1988 or 1998 studies. The slope and intercept values for the 12 μm channel are varied but restrained so that the resulting gamma parameter, g, generally increases with increasing temperature and has realistic values, i.e. $0 < g < 4$, over the entire sea surface temperature range.

First only the intercept value, $I_{11}$, is varied with the parameters $S_{11}$ and $S_{12}$ and $I_{12}$ provided from the 1988 study. Figs. 4 & 5 show the effect of adding a small offset, c, to the intercept $I_{11}$ obtained from the 1988 study. In Fig. 4, g(max) corresponds to the maximum temperature difference, $T_{11} - T_{12}$, resulting from water vapor absorption, as plotted in Fig. 1, and g(0) represents the minimum temperature difference, $T_{11} - T_{12} = 0$. The three different envelopes correspond to three

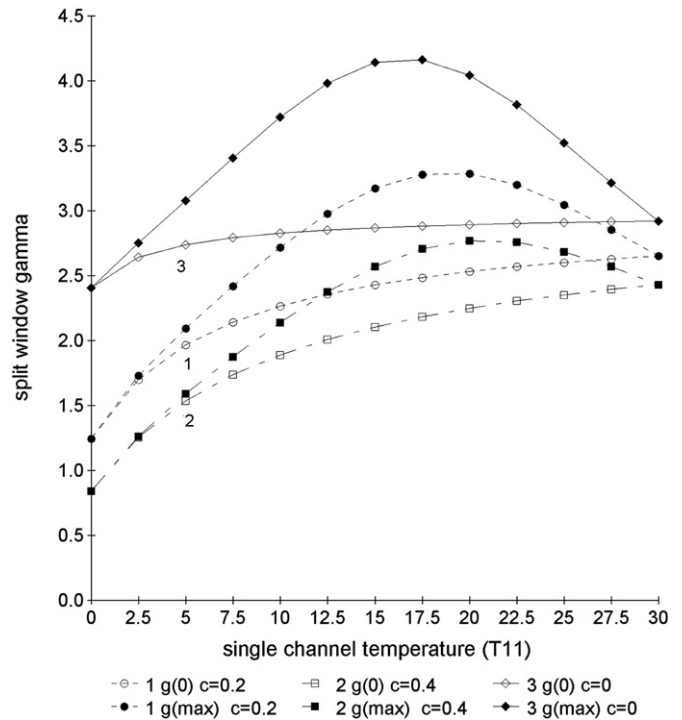**Fig. 4.** Gamma vs. $T_{11}$. The three envelopes show the effect of adding an offset, c, to the intercept, $I_{11}$, while the single channel slopes, $S_{11}$ & $S_{12}$ are constant. The single channel slope and intercept values are those developed in the 1988 study, based on simulation data. Here and in the following graphs, the low and high water vapor curves are identified with open and solid markers, respectively.

different values of the offset to the intercept, c. Generally, decreasing the offset, c, increases the magnitude of the gamma parameter. In Fig. 5, g(T1) and g(T2) are the gamma values at the temperatures provided in Table 1. These temperatures represent respectively the
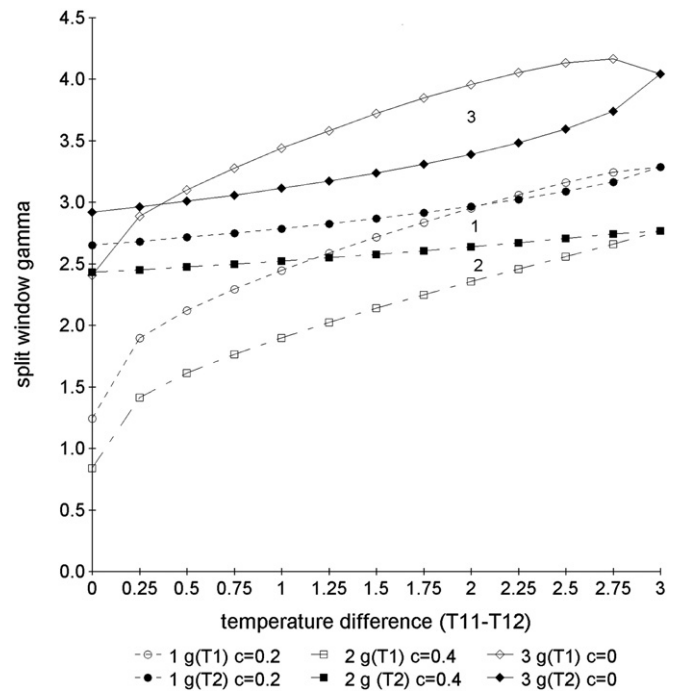
**Fig. 5.** Gamma vs. $T_{11} - T_{12}$. The three envelopes show the effect of adding an offset, c, to the intercept, $I_{11}$, while the single channel slopes, $S_{11}$ & $S_{12}$ are constant. The single channel slope and intercept values are based on the 1988 study referenced in the text. Envelope #1 approximates the QSST algorithm.
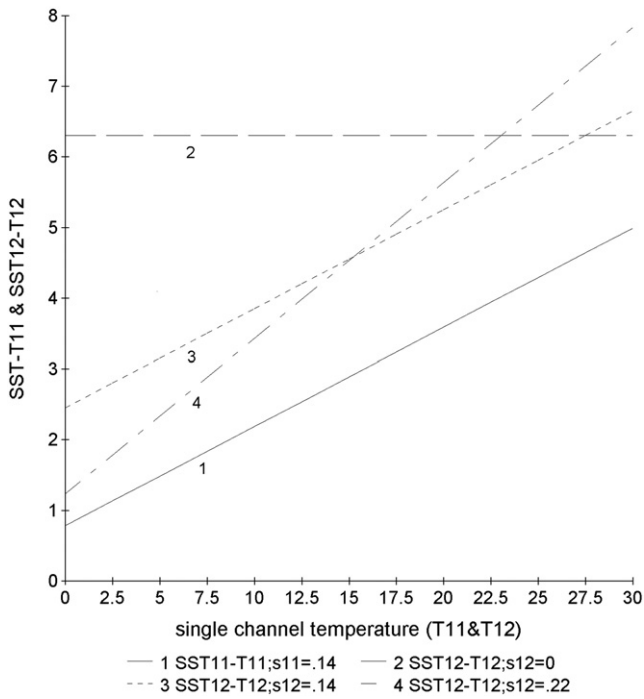
**Fig. 6.** Single channel SST algorithms ($SST_I - T_I$) vs. $T_{11}$. The curves represent four examples of simulated single channel SST algorithms applied in this study. Curve 1 is derived from simulations performed in the 1998 study referenced in the text while the remaining 3 curves are simulations developed in this study.



**Fig. 7.** Gamma as a function of $T_{11}$ for three envelopes defined with different values of the single channel slope parameter, $S_{12}$, such that the ratio parameter $R > = 0$. Envelope #3 represents a type #4 algorithm as described in Section 4 of the text with $R = 1$. Envelope #1 represents the NLSST with $S_{11} = S_{12}$ and $R = 0$.

minimum and maximum 11 μm channel temperatures associated with a given value of the temperature difference, $T_{11} - T_{12}$. As before, the three envelopes correspond to three different values of the offset parameter c. It should be noted that with the intermediate intercept offset, $c = 0.2$, the high and low temperature curves cross at an intermediate value of $T_{11} - T_{12}$, forming a narrow envelope especially for high values of $T_{11} - T_{12}$. This example represents the QSST approximation, described in the previous section, where the temperature correction, $SST-T_{11}$, is a quadratic function of the temperature difference, $T_{11} - T_{12}$.

The application of the offset, c, has an alternative interpretation when it is applied to actual data. The 1988 study, using simulation data, describes a procedure for minimizing the error of the GNLSST relative to the measured SST, after the single channel slope and intercept parameters have been computed. A small addition, c, is applied to the temperature measurement, $T_{11}$.

The value of the parameter c is adjusted to minimize the temperature error, $\sum (GNLSST - SST)^2$, statistically. This same procedure is also applied in the 1998 study. In terms of gamma, adding c to one of the temperatures, $T_{11}$ or $T_{12}$ is equivalent to adding c to one of the intercept parameters. In the 1988 study, it was found that the value of c which minimizes the error of the GNLSST, when applied to simulation data, is 0.2, which is depicted with the middle envelope in Figs. 4 & 5. Thus the most accurate GNLSST solution, obtained from the 1988 simulation data, approximates the QSST algorithm. This result was also found to be true in the 1998 study as depicted in Fig. 11. Interestingly, the first differential absorption algorithm used operationally at NOAA/NESDIS with NOAA-7 satellite data in 1981 was a QSST algorithm, which was based on simulation studies performed at that time (Kidwell, 1995). Subsequently, it was found that the QSST algorithm resulted in significant errors when applied to open ocean satellite data. It was replaced three months after its implementation with the MCSST.

Next, the behavior of gamma is explored when both the slope and intercept values, $S_{12}$ & $I_{12}$, are varied. The parameters, $S_{11}$ & $I_{11}$ are constants obtained from the 1998 simulation data. (Use of the simulation values is arbitrary since the values derived from the open ocean satellite data could also be applied here.) The $S_{12}$ parameter is assigned specific
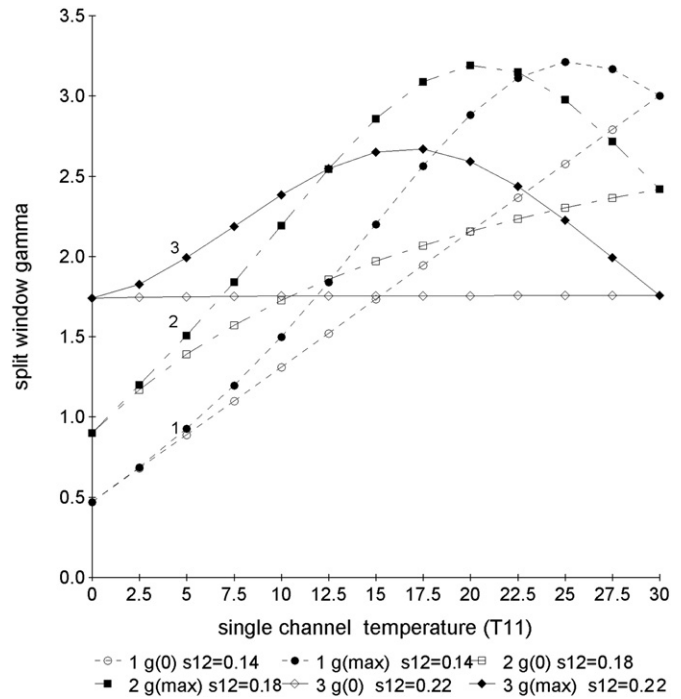
values (0, 0.10, 0.14, 0.18, and 0.22) while the $S_{11}$ slope parameter has a value of 0.14. The $I_{12}$ parameters are then chosen so that the magnitude of the resulting gamma parameter is realistic in terms of providing a correction for atmospheric absorption. The choices also demonstrate some of the special conditions described in Section 4. Fig. 6 shows the
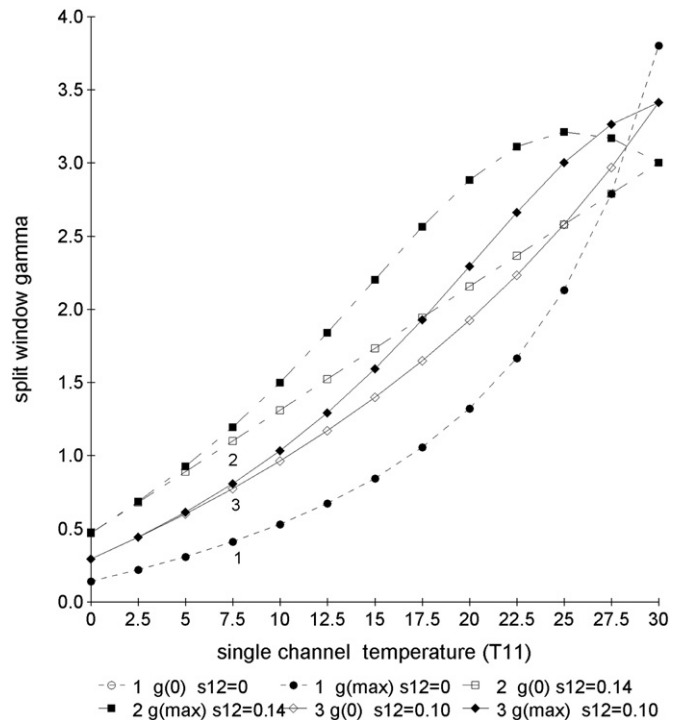


**Fig. 8.** Gamma as a function of $T_{11}$ for three envelopes defined with different values of the single channel slope parameter, S12, such that the ratio parameter $R < = 0$. Envelope #1 converges to a curve representing algorithm type #2 as described in Section 4 of the text. Envelope #2 represents the NLSST with $S_{11} = S_{12}$.

temperature dependence of the single channel algorithms $SST_{11} - T_{11}$ and $SST_{12} - T_{12}$ resulting from the application of these parameter values.

Figs. 7 & 8 demonstrate the temperature dependence of the GNLSST gamma parameter with three envelopes derived from three different values of the $S_{12}$ slope parameter. These figures differ in the choice of the single channel slope parameters. In the former they are chosen so that $S_{12} - S_{11} \geq 0$ while in the latter $S_{12} - S_{11} <= 0$. Figs. 9 and 10 are similar to Figs. 7 and 8 except that the abscissa is changed from single channel temperature measurement to sea surface temperature as defined with Eq. 8. This transformation is achieved with a straight forward interpolation procedure. It is noticed that in Figs. 7 and 8, the curves forming the envelopes converge as the measured $T_{11}$ temperature approaches 30 °C, although they do not converge in Figs. 9 and 10 as the sea surface temperature approaches the same value. This is a consequence of the supposition that the amount of atmospheric absorption is severely constrained as the satellite measured temperatures approach 30 °C, as explained in Section 3. This constraint does not apply to sea surface temperature. Also, the low moisture curves, g(0), in these figures are unchanged in Figs. 7 and 9 as well as Figs. 8 and 10. This results from the fact that the low moisture curves are obtained assuming $T_{11} = T_{12}$. With this condition, the single channel temperature measurement is the sea surface temperature. Comparing envelope #1 in Figs. 7 and 9, one sees that the curves merge together in Fig. 9 to form a straight line, demonstrating that gamma is a linear function of SST, which is the NLSST solution. Comparing Figs. 9 and 10, which depict gamma as a function of SST, one sees that when the ratio parameter, R, is positive, the curves and envelopes have a concave shape but when $R < 0$ the curves are convex. Also, with $R > 0$, the high moisture curves provide the greatest gamma values while the opposite is true when $R < 0$. As is demonstrated in the conclusion, solutions with $R >= 0$ should be expected in data sets containing a large range of temperature and moisture conditions while solutions with $R < 0$ may occur in regional or local scale data sets. Finally, Fig. 11 plots the envelopes associated with three different $S_{12}$ slope values as a function of the $T_{11} - T_{12}$ temperature difference. The broad envelope #1 represents the NLSST approximation, $S_{11} = S_{12}$ and $R = 0$. The high temperature curve, g(T2), yields the highest gamma values. Envelope #2 demonstrates the gamma dependence when the ratio parameter, R, is unity. In this case, the low temperature curve, g(T1), yields the higher gamma values. Envelope #3 is defined using the slope and intercept values obtained from the 1998 study. This envelope shows the high and low temperature curves crossing, demonstrating the QSST approximation.

## 6. Practical considerations resulting from this study

The mathematical properties of the GNLSST have been discussed in this study. It is found that the associated gamma parameter dependence on satellite measured temperature and water vapor absorption varies greatly, depending on the difference between the single channel SST algorithms, $SST_{11}$ and $SST_{12}$. The single channel algorithms obtained from two data sets developed in the 1998 study have been applied to this model. The simulated channel measurements and associated single channel SST algorithms provide a GNLSST solution which approximates the QSST. On the other hand, the open ocean satellite measured data provides a GNLSST solution which approximates the NLSST. Further, the individual data points are, for the most part, enclosed within the corresponding envelopes as shown in Figs. 2 & 3. The question of why such dissimilar solutions are obtained with these two data sets is addressed in the Conclusion.

The ability of the GNLSST to reduce satellite derived SST temperature errors by transforming in this manner, speaks to its robustness as a differential absorption algorithm for measuring SST. However, the GNLSST solution involves a level of complexity not present in the simpler algorithms, i.e. the MCSST, the NLSST and the QSST described previously. Operationally, a multiple term expression provides a satellite estimate
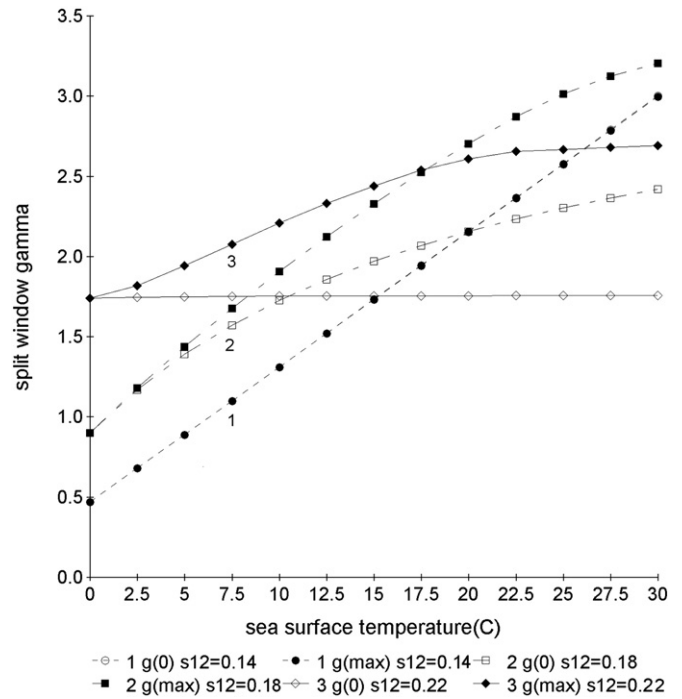


**Fig. 9.** Gamma as a function of SST for three envelopes having different single channel slope parameters, $S_{12}$, such that the ratio parameter $R >= 0$. Envelope #1 converges to a straight line representing the NLSST with $S_{11} = S_{12}$. Envelope #3 represents algorithm type #4 as described in Section 4 of the text.

of SST, such as:

$$SST = a + b * T_{11} + \{c * g + d\} * (T_{11} - T_{12}) + e * (T_{11} - T_{12}) * \{sec\Phi - 1\} \quad (19)$$

Here the coefficients a, b, c, d and e are obtained by multiple linear regression on a large data set of satellite measurements and sea surface
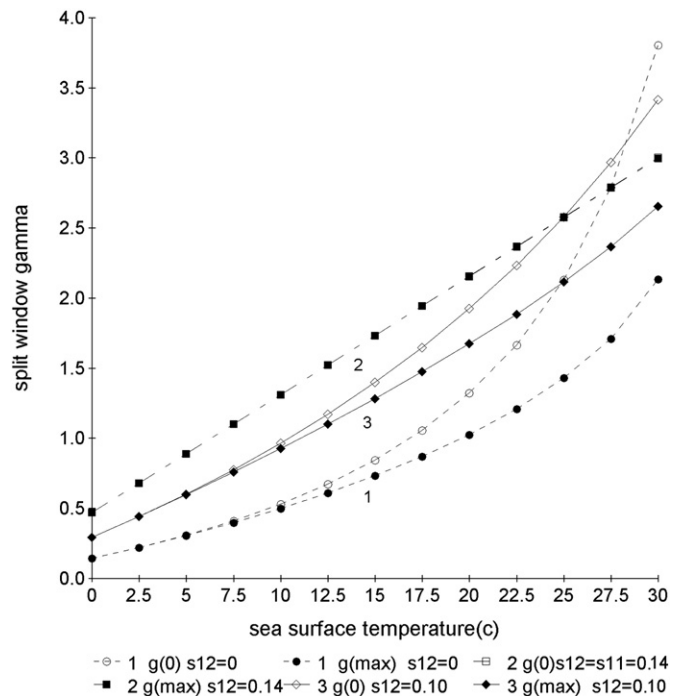


**Fig. 10.** Gamma vs. SST for three envelopes defined with different single channel slope values, S12, such that the ratio $R <= 0$. Envelope #2 converges to a straight line with $R = 0$, representing the NLSST. Envelope #1 represents algorithm type #2 as described in Section 4 of the text.
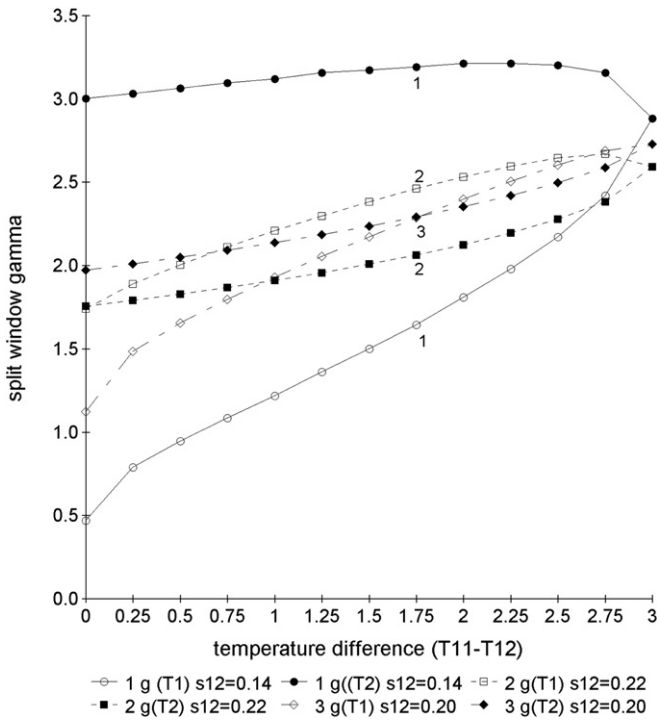
**Fig. 11.** Gamma vs. $T_{11} - T_{12}$ for three envelopes formed using different values for the single channel slope parameter, $S_{12}$. The parameters T1 and T2 correspond to the temperature values given in Table 1 of the text. Envelope #3 approximates the QSST and is obtained with both single channel slope values ($S_{11}$ & $S_{12}$) derived in the 1998 study. Envelope #1 represents the NLSST while envelope #2 represents algorithm type #4 as described in Section 4 of the text.

temperature measurements, such as provided by drifting buoys. The parameter, g, is the temperature dependent component of the gamma parameter defined with Eq. 13 and secΦ is the satellite zenith angle measured at the surface. Thus the MCSST is obtained through a regression with c = 0 and the NLSST is obtained with g = $SST_0$, an initial estimate of the sea surface temperature. The coefficients c and d correspond to those in Eq. 16. The QSST is obtained with g = $T_{11} - T_{12}$. The GNLSST is obtained through a regression with d = 0. However g is a function of the single channel algorithms, $SST_{11}$ and $SST_{12}$. A separate regression must be performed to define these algorithms before Eq. 19 can be applied. Further, if the adjustable offset, described in Section 5, is included in the calculation of g, a further complication arises. In the 1998 study, it was found that this parameter was not needed when the GNLSST was developed from the global open ocean satellite data set. If this is generally true, it would simplify computing a global GNLSST algorithm with Eq. 19. However, regional GNLSST algorithms may require the use of an offset.

Another factor favoring the NLSST is that the gamma parameter is a linear function of the underlying SST. However, one need not use satellite measurements to define an initial estimate of SST. Rather, an analyzed field of sea surface temperatures can be used to define the initial estimate, $SST_0$. Various global analyzes of SST at different resolution are available for this purpose (Brasnett, 2008; Donlon et al., 2012; Reynolds et al., 2007). This has the effect of making the NLSST gamma parameter independent of various satellite measurement errors. Consequently, the impact of satellite measurement errors on the final NLSST estimate of sea surface temperature is considerably less, perhaps 1/3 less, than is the case with the GNLSST (May, 1993). It is demonstrated in Fig. 3 that the NLSST provides a reasonable approximation to the GNLSST gamma parameter when derived from a global data set of open ocean satellite measurements. Because of the elevated impact of measurement errors on the GNLSST, the NLSST has become the

algorithm of choice for measuring SST in the remote sensing community over the past 25 years.

However, it has been demonstrated in this study that the GNLSST yields the NLSST solution only when the slope parameters, $S_{11}$ & $S_{12}$ of the single channel SST algorithms are equal. This generally is not the case so that the application of the NLSST introduces certain errors relative to the GNLSST algorithm. It is seen in Fig. 3 that the open ocean gamma parameter has a small amount of scatter at high SST values resulting from a variable amount of atmospheric absorption by water vapor. Additionally, the envelope curves are not linear but have a slight concave curvature. These effects are not accounted for with the linear NLSST algorithm. Also, many uses of the NLSST algorithm, including NOAA/NESDIS, have assumed that the intercept of the NLSST gamma parameter is zero. Yet, Eq. 17 specifies that the intercept should be non-zero. The impact of these potential sources of errors in the application of the NLSST algorithm can be estimated with the model that has been developed in this study.

In the following development, it is assumed that, in the absence of satellite measurement errors, the GNLSST represents the actual SST and the NLSST errors are measured relative to the GNLSST. This assumption may be reasonable in view of the robustness of the GNLSST, as described previously, and because the GNLSST is derived directly from radiative transfer theory. Various forms of the NLSST are evaluated, to determine which best matches the GNLSST. A version of the NLSST, in which g is a quadratic function of SST, is considered to account for the concave curvature of the GNLSST gamma parameter as a function of SST. Linear NLSST algorithms with different intercept values are also evaluated. Given the intercept, d, a regression procedure is applied to determine the optimal slope value, c, which minimizes the error of the NLSST relative to the GNLSST:

$$\sum_n (T_{11} + g*(T_{11} - T_{12}) - GNLSST)^2 = \min \qquad (20)$$

The parameter g is defined with Eq. 16 and $T_{11} - T_{12} = \Delta T_{max}$. The summation is over the 13 temperature intervals of $T_{11}$ ranging from 0 to 30 °C. This procedure yields an initial value for slope, c in Eq. 16. However at high SST values, g is likely to exceed the maximum GNLSST gamma parameter value of approximately 2.5. The errors of the associated NLSST algorithm can be reduced by limiting or capping g at a value of approximately 2.5, as is demonstrated in Fig. 12.

The resulting RMS errors and slope parameters of the NLSST, using four different values of the intercept parameter, are given in Table 2. The associated regression is designated as non-iterative. It is interesting to note that NOAA/NESDIS similarly limits g in its operational processing by capping the initial SST estimate used to define g at 28 °C (Kidwell, 1995). The RMS error associated with the MCSST algorithm is included for comparison.

A second or iterative regression is performed which minimizes Eq. 20 as before except that all data intervals for which g exceeds the threshold value are excluded from the regression. This is done so that the large errors associated excessively large gamma values do not dominate the regression computations. However, all temperature intervals are included in the computation of RMS errors shown in Table 2. It is seen that the iterative regression considerably reduces the errors associated with the NLSST algorithms. It should be noted that the iterative regression increases the slope parameter, c, which may result in the need for an additional iteration.

Including an intercept parameter in the formulation of the linear NLSST gamma parameter increases accuracy and reduces the magnitude of the slope parameter. The primary benefit of a quadratic version of the NLSST (QNLSST) is that it eliminates the need for an iterative procedure. Generally, the errors listed in Table 2 underestimate the true errors since the scattering of the GNLSST gamma due to water vapor absorption is not fully represented. Additionally, the effect of errors in the initial SST
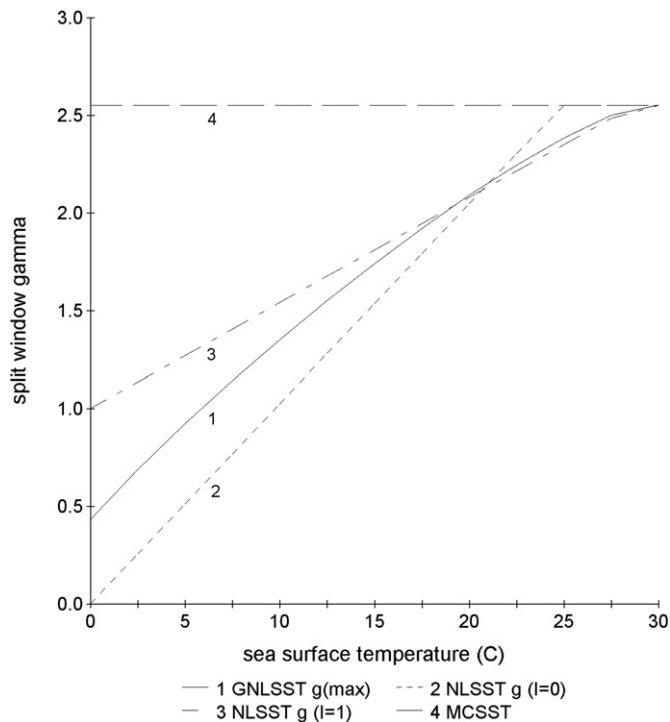
**Fig. 12.** The GNLSST gamma and NLSST gamma vs. SST. The NLSST gamma is computed with two different intercept values, I. The MCSST gamma is shown for comparison. The single channel slope and intercept values which define curve #1 are obtained from actual NOAA 14 satellite measurements used in the 1998 study. Curves 2 & 3 are obtained with the iterative regression procedure described in Section 6 of the text.

**Table 2**
Coefficients and RMS errors of various NLSST algorithms.

|  |  | Linear NLSST | Linear NLSST | | | QNLSST | MCSST |
|---|---|---|---|---|---|---|---|
| Regression | Intercept | 0 | 0.50 | 0.75 | 1.0 | 0.43 | 2.5 |
| Non-iterative | RMS | 0.39 °C | 0.22 °C | 0.16 °C | 0.16 °C | 0.10 °C | 0.55 °C |
| Iterative | RMS | 0.24 °C | 0.12 °C | 0.10 °C | 0.13 °C | – | – |
| Non-iterative | Slope | 0.090 | 0.071 | 0.062 | 0.052 | – | 0 |
| Iterative | Slope | 0.102 | 0.078 | 0.066 | 0.054 | – | – |

estimate, $SST_0$, used to define the NLSST gamma parameter is not considered here but is described in some detail in the 1998 study.

Normally, both the slope and intercept would be derived from a regression analysis as is implied with Eq. 19. In this case, one finds that the non-iterative and iterative regressions yield intercept values of 0.99 and 0.77 respectively, which are closely approximated in Table 2. In this example, it appears that the iterative regression procedure is just as applicable and beneficial when both the slope and intercept are derived by regression as it is when only the slope is computed.

## 7. Conclusion

The GNLSST algorithm has been derived from radiative transfer theory with some approximations. It is demonstrated that the solution can take many forms depending on the temperature dependence of the single channel algorithms, $SST_{11}$ & $SST_{12}$. The remote sensing community, however, has embraced one approximate solution, the NLSST, for measuring sea surface temperature in the open ocean due to its simplicity and low noise characteristics. An obvious question is whether the NLSST is a good approximation to the GNLSST over time and with different satellite instrumentation. As described in the Introduction, although the NLSST performed well with open ocean data in the 1998 study, with a simulation data set of satellite measurements, it was found that the

NLSST was a poor approximation to the GNLSST algorithm. The NLSST resulted in greater errors when compared to radiosonde surface air temperature measurements. In order to answer the previous question, one needs to explain the curious results described above.

It was implied in the 1998 study that the different findings obtained with the simulation and open ocean data sets resulted from a fundamental difference in the temperature measurements themselves. This assumption may not be correct. It is true that the simulation temperatures are derived from an old radiative transfer model which does not account for nonzero surface reflectivity effects. Yet the model does include detailed computations of absorption by water vapor and the uniformed mixed gases (Weinreb and Hill, 1980). All computations are performed at nadir so that surface reflectivity effects in the 11 and 12 μm spectral bands should be minimal (Dash and Ignatov, 2008). The open ocean satellite measurements do include small errors resulting from instrumental noise and perhaps residual cloud contamination which are not present in the simulation data. However the simple regression procedures that provide the single channel parameters ($SST_{11}$ and $SST_{12}$), which are applied in the GNLSST algorithm, should be insensitive to these noise factors. These are minor compared to the variation of temperature measurements resulting from variable water vapor absorption. Therefore, it is suggested that the different results obtained with the GNLSST algorithm is not a consequence of the fact that one data set is composed of simulation data and the other is composed of open ocean satellite measurements. Rather, the differing results may be a consequence of the fact that the two data sets consist of totally different distributions of data. The simulation data set consists of simulated AVHRR temperatures derived from a 115 radiosonde soundings representing a range of typical marine conditions around the globe. The open ocean data set consists of over 4000 NOAA-14 AVHRR satellite temperature measurements combined with in-situ drifting buoy measurements, providing nearly complete global coverage. It is the distribution of temperatures and water vapor within each data set that determines the form of the GNLSST solution.

The sensitivity of the GNLSST solution to the distribution of the temperature measurements is explained with Fig. 13. Here the GNLSST, derived from the open ocean data in the 1998 study, is plotted against the split-window temperatures ($T_{11}$ & $T_{12}$), developed with the water vapor model described in Section 3. In this application, any reasonable SST algorithm such as a MCSST or QSST algorithm would provide similar curves. The two curves associated with each spectral temperature, resulting from minimum and maximum water vapor absorption, form an envelope. The $T_{11}$ and $T_{12}$ envelopes have been separated by 5° for clarity. The central curve in the $T_{12}$ envelope represents an average water vapor condition with $\Delta T = \Delta T_{max}/2$ at each temperature interval, with $\Delta T_{max}$ defined in Eq. 12. The flattening of the non-zero water vapor curves at high temperatures is a consequence of the constraint on $\Delta T$ as described in Section 3. Individual data points within a given data set of split-window temperature measurements paired with in-situ measurements of SST should be contained within the appropriate envelopes. Fig. 13 demonstrates that the single channel SST algorithms, $SST_{11}$ & $SST_{12}$, which define the GNLSST solution, are sensitive to the distribution of data within the envelopes. If the data is approximately equally distributed between 0 and 25 °C and scattered between the two curves forming each envelope due to varying water vapor absorption, then the linear regression slope parameters, $S_{11}$, and $S_{12}$, defined with Eq. 10, will be positive. If the data is restricted to between 20 and 30 °C then these parameters will be negative. If the data is equally distributed between 15 and 25 °C then the slope parameters may be close to zero, as represented by the straight zero absorption lines forming the base of each envelope.

Fig. 14 illustrates the gamma parameter dependence on temperature for each of these three data distribution scenarios. It is assumed that average water vapor conditions apply so that the mean curve, shown in the $T_{12}$ envelope of Fig. 13, represents the mean of the data points as a function of temperature. The linear regression, defining $SST_{11}$ and
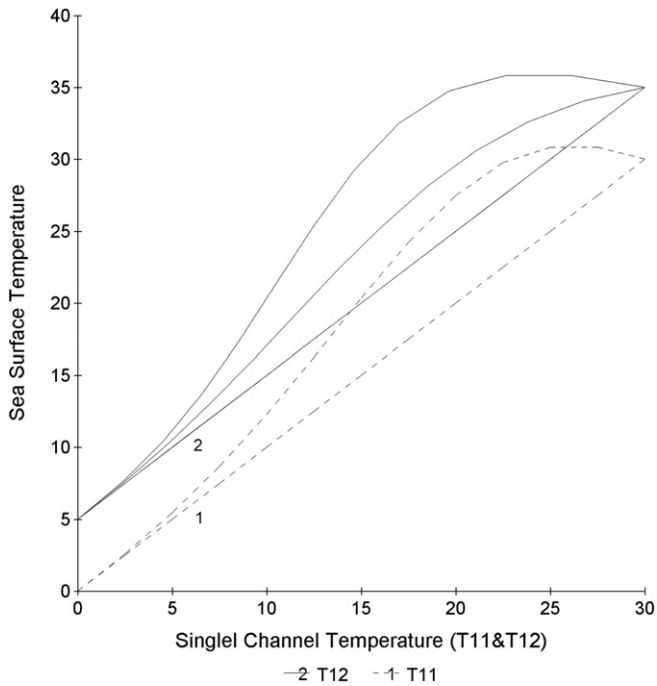
**Fig. 13.** An estimate of SST vs.$T_{11}$ and $T_{12}$, using a GNLSST algorithm developed with open ocean data in the 1988 study. $T_{11}$ and $T_{12}$ values are applied assuming minimum and maximum water vapor conditions as described in Section 3. The resulting $T_{11}$ and $T_{12}$ envelopes are separated by 5° on the ordinate axis for clarity. A linear regression using data within these envelopes provide the single channel algorithms, $SST_{11}$ and $SST_{12}$, which define the GNLSST gamma. The medium curve in the $T_{12}$ envelope represents average water vapor conditions.
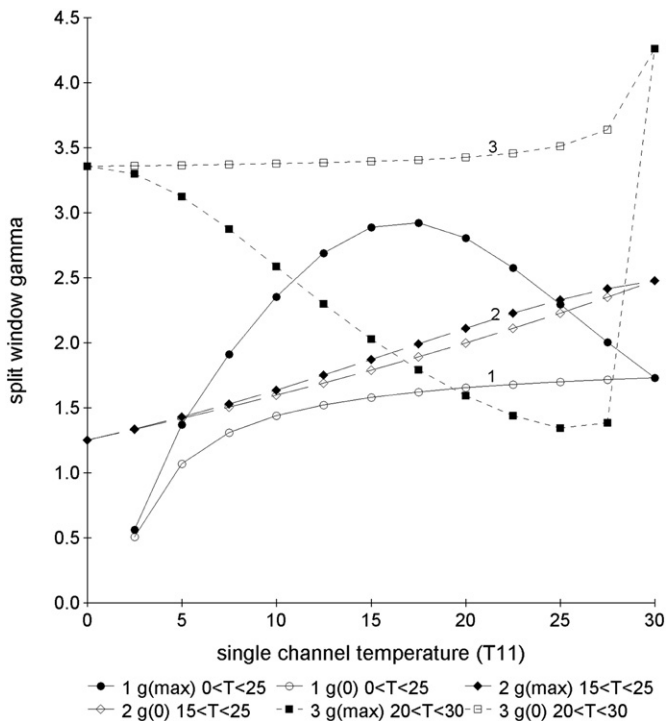


**Fig. 14.** Gamma vs. $T_{11}$ for three envelopes, obtained assuming average water vapor conditions. The $SST_{11}$ and $SST_{12}$ parameters applicable in each envelope are derived by linear regression using a different distribution of temperature data. Envelopes 1, 2 and 3 assume respectively uniform temperature distributions $0 < T_{11} < 25$, $15 < T_{11} < 25$, and $20 < T_{11} < 30$. The corresponding slope parameters, $S_{11}$ and $S_{12}$, associated with each envelope, are respectively, (0.14, 0.22), (0.037, 0.025), and (−0.31, −0.41).

$SST_{12}$ with Eq. 10, provides the best fit to the mean curve within the appropriate temperature range. The envelopes shown in Fig. 14 are not representative of what would be obtained with actual data and are shown for illustrative purposes only. Envelope 1 is somewhat representative of a Type 6 QSST algorithm while envelopes 2 and 3 are best approximated as Type 2 and Type 7 algorithms as described in Section 4. Other distributions of data may result in different types of solutions. For instance, if the data distribution is approximately uniform over the entire temperature range from 0 to 30 °C, then the GNLSST solution is best represented with a NLSST Type 5 algorithm.

The sensitivity of the GNLSST algorithm to the data distribution implies that no single algorithm for measuring SST is optimal for all users of split-window data. To answer the question presented at the beginning of this section, an NLSST type solution may provide consistent results with global data obtained with different polar orbiting AVHRR type instruments because the data distribution is consistent over time. However, regional users of satellite data may find that a global NLSST algorithm is not appropriate for their application. Modern satellite simulation data could be used to evaluate alternative regional algorithms. Whether a GNLSST algorithm or a global NLSST algorithm provides the most accurate results in a given application can only be determined by each user individually. With all multi-channel SST algorithms, perhaps particularly with regional GNLSST algorithms, it is very important that the dependent data set, used to derive the algorithm coefficients, include the entire range of temperature and moisture conditions which will be found in subsequent independent data sets.

One problem involved with the use of the GNLSST is the elevated noise associated this algorithm as compared with the NLSST, which is discussed in Section 6. One method of reducing this noise is to apply a smoothing procedure. The GNLSST gamma parameter, defined with Eq. 8 & 13, could be smoothed spatially and temporally. If the resulting resolution was equivalent to the resolution of the temperature analysis used to define the NLSST gamma value, $SST_0$, much of the elevated noise would probably be removed. Another possibility is to apply modern satellite simulation data in the computation of the GNLSST. A parallel simulation measurement, associated with each satellite measurement of split-window data, is computed as part of the current operational processing at NOAA. The process uses a global analysis of SST and a Global Forecast System upper-air fields as input to a fast radiative transfer model (Liang and Ignatov, 2011). Consequently, in the derivation of the GNLSST, one could apply the simulation temperature measurements to define gamma while using the actual satellite measurements to derive the SST estimate as represented with Eq. 8 and 19. This procedure should remove any correlation between the errors associated with the computation of gamma and those associated with the satellite measurements applied in the GNLSST algorithm. This should significantly reduce the overall noise of the algorithm. Given the pervasive nature of residual satellite measurement errors, whether the GNLSST can match or exceed the accuracy of the global NLSST algorithm, using either of these noise reduction procedures, remains an open question.

## Acknowledgments

## References

Anding, D., Kauth, R., 1970. Estimation of sea surface temperature from space. Remote Sens. Environ. 1 (4), 217–220.

Brasnett, B., 2008. The impact of satellite retrievals in a global sea-surface-temperature analysis. Q. J. R. Meteorol. Soc. 134 (636), 1745–1760.

Cayula, J.F.P., May, D.A., McKenzie, B.D., Willis, K.D., 2013, June. VIIRS-derived SST at the Naval Oceanographic Office: From evaluation to operation. SPIE Defense, Security, and Sensing. International Society for Optics and Photonics, p. 87240S.

Cracknell, A.P., 1997. Advanced Very High Resolution Radiometer AVHRR. CRC Press.

Dash, P., Ignatov, A., 2008. Validation of clear-sky radiances over oceans simulated with MODRTRAN4.2 and global NCEP GDAS fields against nighttime NOAA15-18 and MetOp-A AVHRR data. Remote Sens. Environ. 112, 3012–3029.

Donlon, C.J., Martin, M., Stark, J., Roberts-Jones, J., Fiedler, E., Wimmer, W., 2012. The operational sea surface temperature and sea ice analysis (OSTIA) system. Remote Sens. Environ. 116, 140–158.

Hosoda, K., Qin, H., 2011. Algorithm for estimating sea surface temperatures based on Aqua/MODIS global ocean data. 1. Development and validation of the algorithm. J. Oceanogr. 67, 135–145.

NOAA Polar Orbiter Data Users Guide:(TIROS-N, NOAA-6, NOAA-7,NOAA-8, NOAA-9, NOAA-10, NOAA-11, NOAA-12, NOAA-13, and NOAA-14) Appendix E. In: Kidwell, K.B. (Ed.), National Oceanic and Atmospheric Administration, National Environmental Satellite, Data, and Information Service. Satellite Data Services Division, National Climatic Data Center.

Kilpatrick, K.A., Podesta, G.P., Evans, R., 2001. Overview of the NOAA/NASA advanced very high resolution radiometer pathfinder algorithm for sea surface temperature and associated matchup database. J. Geophys. Res. 106 (C5), 9179–9197.

Kumar, A., Minnett, P.J., Podestá, G., Evans, R.H., 2003. Error characteristics of the atmospheric correction algorithms used in retrieval of sea surface temperatures from infrared satellite measurements: global and regional aspects. J. Atmos. Sci. 60 (3), 575–585.

Le Borgne, P., Legendre, G., Marsouin, A., Péré, S., Roquet, H., 2013, June. OSI-SAF operational NPP/VIIRS sea surface temperature chain. SPIE Defense, Security, and Sensing. International Society for Optics and Photonics, p. 87240T.

Liang, X.-M., Ignatov, A., 2011. Monitoring of IR Clear-Sky Radiances over Oceans for SST (MICROS). J. Atmos. Ocean. Technol. 114, 1228–1242.

May, D.A., 1993. Global and regional comparative performance of linear and non-linear satellite multichannel sea surface temperature algorithms. Tech. Rep. NRL/MR/7240-93-7049. Nav. Res. Lab., Stennis Space Cent., Miss.

May, D.A., Holyer, R.J., 1993. Sensitivity of satellite multichannel sea surface temperature retrievals to the air-sea temperature difference. J. Geophys. Res. 98 (C7): 12567–12577. http://dx.doi.org/10.1029/93JC00913.

McClain, E.P., Pichel, W.P., Walton, C.C., 1985. Comparative performance of AVHRR based multichannel sea surface temperatures. J. Geophys. Res. 90, 11587–11601.

McMillin, L.M., 1975. Estimation of sea surface temperatures from two infrared window measurements with different absorption. J. Geophys. Res. 80 (36), 5113–5117.

McMillin, L.M., Crosby, D.S., 1984. Theory and validation of the multiple window sea surface temperature technique. J. Geophys. Res. Oceans (1978–2012) 89 (C3), 3655–3661.

Merchant, C.J., Le Borgne, P., Marsouin, A., Roquet, H., 2008. Optimal estimation of sea surface temperature from split-window observations. Remote Sens. Environ. 112 (5), 2469–2484.

Minnett, P.J., 1986. A numerical study of the effects of anomalous North Atlantic atmospheric conditions on the infrared measurement of sea-surface temperature from space. J. Geophys. Res. 91, 8509–8521.

Minnett, P.J., 1990. The regional optimization of infrared measurements of sea surface temperature from space. J. Geophys. Res. Oceans 95 (C8), 13497–13510.

Minnett, P.J., Evans, R.H., 2009. MODIS sea-surface temperatures (paper presented at GHRSST User Symposium, Santa Rosa, Ca., 28–29 May).

Minnett, P.J., Brown, O.B., Evans, R.H., Key, E.L., Kearns, E.J., Kilpatrick, K., ... Szczodrak, G., 2004. Sea-surface temperature measurements from the Moderate-Resolution Imaging Spectroradiometer (MODIS) on Aqua and Terra. Geoscience and Remote Sensing Symposium. 7, pp. 4576–4579 IGARSS'04. Proceedings. 2004 IEEE International. (IEEE).

Petrenko, B., Ignatov, A., Kihai, Y., Stroup, J., Dash, P., 2014. Evaluation and selection of SST regression algorithms for JPSS VIIRS. J. Geophys. Res.-Atmos. 119 (8), 4580–4599.

Prabhakara, C., Dalu, G., Hunde, V.G., 1974. Estimation of sea surface temperature from remote sensing in the 11- to 13 μm window region. J. Geophys. Res. 79 (33), 5034–5044.

Reynolds, R.W., Smith, T.M., Liu, C., Chelton, D.B., Casey, K.S., Schlax, M.G., 2007. Daily high-resolution-blended analyses for sea surface temperature. J. Clim. 20 (22), 5473–5496.

Smith, W.L., Woolf, H.M., Abel, P.G., Hayden, C.M., Chalfant, M., Grody, N., 1974. NIMBUS-5 sounder data processing system. NOAA Tech. Memo., NESS 57 (99 pp).

Stephens, G.L., 1990. On the relationship between water vapor over the oceans and sea surface temperature. J. Clim. 3 (6), 634–645.

Strong, A.E., McClain, E.P., 1984. Improved ocean surface temperatures from space-comparisons with drifting buoys. Bull. Am. Meteorol. Soc. 65 (2), 138–142.

Walton, C.C., 1982. Recent improvements in deriving sea surface temperatures from the NOAA-6 satellite system. IEEE Transactions on Geoscience and Remote Science GE-20 (#3), 404–408.

Walton, C.C., 1988. Nonlinear multichannel algorithms for estimating sea surface temperature with AVHRR satellite data. J. Appl. Meteorol. 27, 115–124.

Walton, C.C., McClain, E.P., Sapper, J.F., 1990. Recent changes in satellite-based multichannel sea surface temperature algorithms. Marine Technology Society Meeting, MTS 90.

Walton, C.C., Pichel, W.G., Sapper, J.F., May, D.A., 1998. The development and operational application of nonlinear algorithms for the measurement of sea surface temperatures with the NOAA polar orbiting environmental satellites. J. Geophys. Res. Oceans 103 (C12), 27999–28012.

Webster, P.J., Clayson, C.A., Curry, J.A., 1996. Clouds, radiation, and the diurnal cycle of sea surface temperature in the tropical western Pacific. J. Clim. 9 (8), 1712–1730.

Weinreb, M.P., Hill, M.L., 1980. Calculation of atmospheric radiances and brightness temperatures in infrared window channels of satellite radiometers. NOAA Tech. Rep., NESS 80.